Journal of
Materials Chemistry B

Accepted Manuscript

This article can be cited before page numbers have been issued, to do this please use: Y. Wang, K. Huang, X. Wu, Y. Ma, D. Song, C. Du and S. Chang, *J. Mater. Chem. B*, 2018, DOI: 10.1039/C8TB00061A.

ROYAL SOCIETY OF CHEMISTRY

rsc.li/materials-b

View Article Online
DOI: 10.1039/C8TB00061A

Graphic abstract

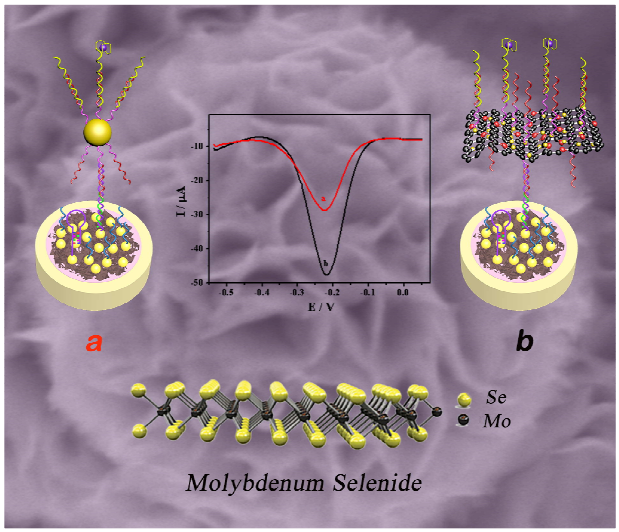

View Article Online
DOI: 10.1039/C8TB00061A

Ultrasensitive supersandwich-type biosensor for enzyme-free amplified microRNA detection based on N-doped graphene/Au nanoparticles and hemin/G-quadruplexes

Yi-Han Wang [a], Ke-Jing Huang [a,*], Xu Wu [b,*], Ying-Ying Ma [a], Dong-Ling Song [a], Chen-Yu Du [a], Su-Huai Chang [a]

[a] *College of Chemistry and Chemical Engineering, Xinyang Normal University, Xinyang 464000, China*

[b] *College of Physics and Electronic Engineering, Xinyang Normal University, Xinyang 464000, China*

*Corresponding author. Tel.: +86-376-6390611

E-mail address: kejinghuang@163.com (K.J. Huang)

View Article Online
DOI: 10.1039/C8TB00061A

ABSTRACT: A simple supersandwich-type biosensor is fabricated for the ultrasensitive determination of microRNAs (miRNAs) using N-doped graphene/Au nanoparticles (NG-AuNPs) and hemin/G-quadruplexes based enzyme-free. In the proposed strategy, AuNPs are deposited on the surface of $MoSe_2$ modified electrode to immobilize the thiol-modified hairpin probe through the strong Au-S bond. When target miRNA is added, capture DNA hybridizes with it and unfolds its stem-and-loop structure. Modification of NG-AuNPs hybrids as the main amplification element hybridize with assistance DNA and the terminus of capture DNA, resulting in the formation of supersandwich structure. Assistance DNA is embedded into hemin/G-quadruplexes complexes in the presence of hemin and K^+ to provide an exceptional current signal for detection of miRNAs. Under the optimized experiment conditions, the detection limit of 0.17 fM is obtained with linear range of 10 fM-1 nM. In addition, the present biosensor shows outstanding selectivity toward mismatched miRNAs. This biosensor platform successfully realized the combination of signal amplification technique with supersandwich structure, providing a promising approach for the detection of miRNA-21 in practical application.

View Article Online
DOI: 10.1039/C8TB00061A

1. Introduction

MicroRNA (miRNA) is endogenous and small non-coding regulatory molecule with about 20-24 nucleotides that play an essential role in the expression of genes.[1,2] MiRNA-21 plays an important role in a plethora of biological functions and diseases including development, cancer, cardiovascular diseases and inflammation.[3] Especially, miRNA-21 level in gastric cancer patients' blood serum is elevated.[4,5] Thus, developing a specific method to sensitively detect miRNA-21 is imperative in clinical cases. To date, various analysis methods have been developed for miRNA detection, such as colorimetric method,[6,7] fluorescence assay,[8-10] surface enhanced Raman scattering,[11,12] surface plasmon resonance[13] and electrochemical biosensor.[14-16] However, many of them required sophisticated and expensive instruments, which limit their practical applications. Electrochemical sensors with the intrinsic advantages of simple, low cost, high sensitivity and rapid response, and have attracted great interest.

To further ameliorate the sensitivity, various amplification strategies are commonly used. Such as rolling circle amplification (RCA),[17,18] polymerase chain reaction (PCR),[19,20] ligase chain reaction (LCR),[21] hybridization chain reaction (HCR),[22,23] catalytic hairpin assembly (CHA)[24] and strand displacement amplification (SDA).[25] Although these amplification strategies show their good performances, but there are still some shortcomings such as complex process of using various tool enzymes, which usually have some defects such as expensive, unstabitily, storage difficulty and special reaction conditions like temperature and pH. So amplification

View Article Online
DOI: 10.1039/C8TB00061A

strategies based on these enzymes require relatively clean samples, limiting the general application of biosensors. Recently, many enzyme-free approaches have been proposed, which can eliminate the unfavorable factors of enzyme.[26]

In recent years, nanomaterials based signal amplification have been widely used to improve the sensitivity of biosensors. Graphene (GR), GR derivatives and GR-like 2D transition-metal dichalcogenides (TMDCs), such as VS_2,[27] MoS_2,[28] and WSe_2[16]. As a typical TMDCs material, $MoSe_2$ is vertically stacked by sandwiched Se-Mo-Se layers with weak Van der Waals interactions.[29] It has been reported $MoSe_2$ has a higher intrinsic electrical conductivity than MoS_2 due to the more metallic nature of Se, and the unsaturated Se-edges in $MoSe_2$ are also found to be electrocatalytically active,[30,31] indicating its more outstanding electrochemical performance. Our group have prepared some biosensors for miRNA detection based on TMDCs and GR.[15,28] In this work, nitrogen-doped graphene (NG) and the flower-like $MoSe_2$ microspheres are selected as supporting substrate owing to their large surface area, superior conductivity, chemical stability and low cost. In addition, NG can be used as substrate to the loading of Au nanoparticles (AuNPs) to fabricat the AuNPs-decorated NG (NG-AuNPs) composites. It is well known that, AuNPs can form links with aptamers through Au-S or Au-NH chemical bonds. Furthermore, NG-AuNPs composites can provide more active sites for the immobilization of DNA probe and enhance electron transfer rate, thus lower the detection limit of proposed assay.

Sandwich-type strategy used in biosensor fabrication usually can greatly increases its specificity and sensitivity. Some works have shown good analytical

View Article Online
DOI: 10.1039/C8TB00061A

performance of sandwich-like graphene-NP structure.[32-34] Herein, a simple, enzyme-free supersandwich-type biosensor is fabricated for miRNA with NG-AuNPs, flower-like $MoSe_2$ microspheres and hemin/G-quadruplexes. The principle of the developed biosensor is shown in Scheme 1. AuNPs are deposited on the $MoSe_2$ modified electrode to immobilize thiol-modified hairpin DNA probe through Au-S bond. 6-mercapto-1-hexanol (MCH) is used as a blocking agent and maintains correct orientation of the ssDNA for sufficient recognition ability. In the presence of miRNA, capture DNA hybridizes with it and unfolds its stem-and-loop structure. Subsequently, DNA-linked NG-AuNPs hybrids are introduce on the modified electrode by hybridizing with capture DNA. After that, DNA-linked NG-AuNPs hybrids initiate the production of DNA supersandwich structure when assistance DNA is added. Finally, assistance DNA is folded into hemin/G-quadruplexes structure in the presence of hemin and K^+ to give a exceptional current response due to the oxidation of Fe(II) in hemin.[35] The fabricated biosensor also presents high sensitivity, simplicity, good selectivity and stability. It may provide one promising assay for miRNA practical analysis and disease diagnostics.

View Article Online
DOI: 10.1039/C8TB00061A

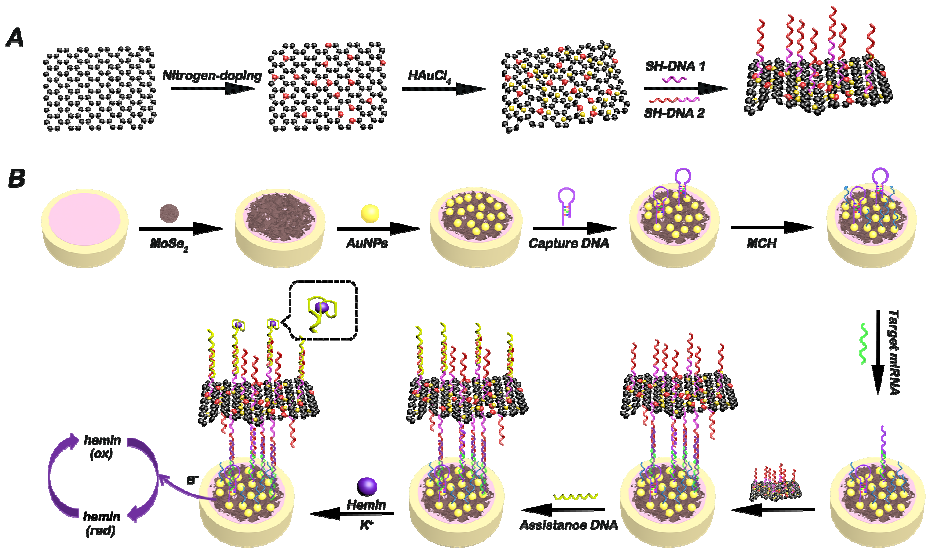

Scheme 1. (A) Preparation of DNA-linked NG-AuNPs hybrids; (B) Fabrication process of the supersandwich-type biosensor for microRNA detection.

2. Experimental section

2.1 Chemicals

Chemicals ($Na_2MoO_4 \cdot 2H_2O$, Se, $NaBH_4$, $HAuCl_4 \cdot 4H_2O$, graphite powder, MCH, and tris-(2-carboxyethyl) phosphine hydrochloride (TCEP) were purchased from Sigma-Aldrich (Shanghai, China). The DNA sequences (purified by HPLC) were prepared by Sangon Biotechnology Co., Ltd. (Shanghai, China). The sequences were showed in Table 1.

Table 1

Sequences of the oligonucleotides.

Oligonucleotides	Sequences
Capture probe	5'-SH-$(CH_2)_6$-TTTTTCAACATCAGTCTGA

View Article Online
DOI: 10.1039/C8TB00061A

	TAAGCTATGCATGATGTTGAATTGC-3’
SH-DNA1	5’-SH-$(CH_2)_6$-TTTTT-3’
SH-DNA2	5’-SH-$(CH_2)_6$-TTTTTGCAATTCAACAT-3’
Assitance DNA	5’-ATGTTGAATTGCTTTTGGGTTGGGCG GGATGGGTGAGAA-3’
MiRNA-21	5’-UAGCUUAUCAGACUGAUGUUGA-3’
Single-base mismatch RNA (smRNA)	5’-UAGCUUAUCAGAAUGAUGUUGA-3’
Three-base mismatch RNA (tmRNA)	5’-UAGCUUGUCAGAAUGAUGAUGA-3’
Non-complementary	5’-CGUAGCGAUUCUACAGGUAAUC-3’

*The underlined letters in capture probe represent the complementary base sequences.

2.2 Apparatus and measurements

Samples were morphologically characterized using a scanning electron microscope (SEM, S-4800, Hitachi, Japan) and transmission electron microscope (TEM, JEM 2100, Japan). Electrochemical measurements were performed on an EC550 electrochemical workstation (Wuhan, Gaoss Union, China). One platinum wire was used as auxiliary electrode and saturated calomel electrode (SCE) as reference electrode.

2.3 Synthesis of flower-like $MoSe_2$ nanoflowers

The $MoSe_2$ microspheres were prepared as follows: 19.6 mmol of Se powder and 6.9 mmol of sodium borohydride were first dissolved in 80 mL mixture of ethanol and

View Article Online
DOI: 10.1039/C8TB00061A

deionized water (1:1 volume ratio) under continuous stirring until clear solution was obtained. Subsequently, 6.8 mmol of sodium molybdate was dispersed in it. The solution was then added in one autoclave and kept at 200 °C for 48 h. The precipitate was centrifugated, washed with water and ethanol, and dried at 60 °C for 12 h under vacuum.

2.4 Preparation of DNA-linked NG/AuNPs composites

Graphene oxide (GO) was first prepared according to reference.[36] The NG sheets were synthesized according to reference.[37] Typically, 60 mg GO was dissolved in 30 mL deionized water (pH 10). 2 mL hydrazine hydrate was added. This solution was continuously stirred for 10 min and heated at 200 °C for 3 h. The black product was obtained after washed with distilled water and dried.

NG-AuNPs was prepared by the reduction of $HAuCl_4 \cdot 4H_2O$ on the NG surface using sodium citrate as the electronating agent. For preparation of the SH-DNA1 and SH-DNA2 modified NG/AuNPs hybrids[38,39]: SH-DNA1 and SH-DNA2 were first dissolved in 20 mM Tris-HCl buffer solution (50 mM sodium chloride, 10 mM magnesium chloride, 10 mM TCEP, pH 7.0), respectively. 10 μL 0.1 mM of SH-DNA1 and SH-DNA2 were then added in 1 mL NG/AuNPs and kept at 4 °C for 16 h. Afterwards, this solution was added in 1 mL of 10 mM PBS (pH 7.0) solution for 48 h at 4 °C. The DNA-linked NG/AuNPs composites were collected by centrifuging under 9000 rpm for 300 s and washed with PBS. Finally, the precipitate was dispersed in 1 mL PBS.

View Article Online
DOI: 10.1039/C8TB00061A

153

154 **2.5 Fabrication of the biosensor**

155 Firstly, the capture probe was annealed at 95 °C for 10 min. The bare GCE was
156 polished with 0.05 μm alumina slurries according to the previous procedure.[15]
157 Subsequently, 8 μL $MoSe_2$ solution (1 mg/mL) was dropped on electrode to get
158 $MoSe_2$/GCE. Then, it was soaked in 0.1% $HAuCl_4$ solution with 0.1 M potassium
159 nitrate to perform electrodeposition of AuNPs under the -0.2 V for 25 s. Afterward, 12
160 μL 20 mM Tris-HCl solution containing 1 μM capture probe was applied on
161 AuNPs/$MoSe_2$/GCE and kept at room temperature for overnight. The capture probe
162 was immobilized on electrode by the strong Au-S[40] and electrostatic interaction with
163 the positively charged AuNPs.[41] After washed with water the GCE was incubated into
164 1 mM MCH for 0.5 h to eliminate nonspecifically adsorbed ssDNA molecules.[42]
165 MiRNA-21 and assistance DNA were dissolved in 10 mM PBS. 8 μL analyte was
166 then modified on the electrode and kept at 37 °C for 50 min under enclosed
167 environment. After rinsing thoroughly with water, 10 μL of DNA-linked NG-AuNPs
168 hybrid was dropped on electrode and kept at room temperature for 80 min. After that,
169 8 μL of 5 μM assistance DNA was applied on electrode and kept at 37 °C for 0.5 h.
170 Finally, the electrode was incubated in 25 mM HEPES buffer solution (200 mM NaCl,
171 20 mM potassium chloride and 1% DMSO, pH 8.0) with 50 μM hemin for 30 min to
172 trigger remaining fragment of assistance DNA to generate G-quadruplex/hemin
173 complexes.

174

View Article Online
DOI: 10.1039/C8TB00061A

3. Results and discussion

3.1 Characterizations

As-prepared material was characterized with SEM and TEM. As displayed in Fig. 1A and B, $MoSe_2$ shows flower-like shapes. The average size of $MoSe_2$ is ~400 nm, which consists of graphene-like thin nanosheets with large surface area, being suitable for aptasensor construction. TEM images are depicted in Fig. 1C and D, demonstrating that the flower-like $MoSe_2$ microspheres are composed of ultra-thin nanosheets, which are well consistent with SEM results. Fig. 1E displays a high-resolution TEM (HRTEM) image of $MoSe_2$ microspheres, which is derived from the circled area in Fig. 1C. The HRTEM image recorded from the standing edges reveals clear lattice spacing of 0.65 nm that corresponds to (002) planes of 2H-$MoSe_2$ (JCPDS Card, No.87-2419).[43] The results of the SEM-energy dispersive X-ray (EDX) are showed in Fig. 1F. It can be seen that the material contains Mo and Se, and no other elements are observed. Besides, the atomic ratio of Se to Mo is 2.03, which agrees with theoretical stoichiometric value of $MoSe_2$.

View Article Online
DOI: 10.1039/C8TB00061A

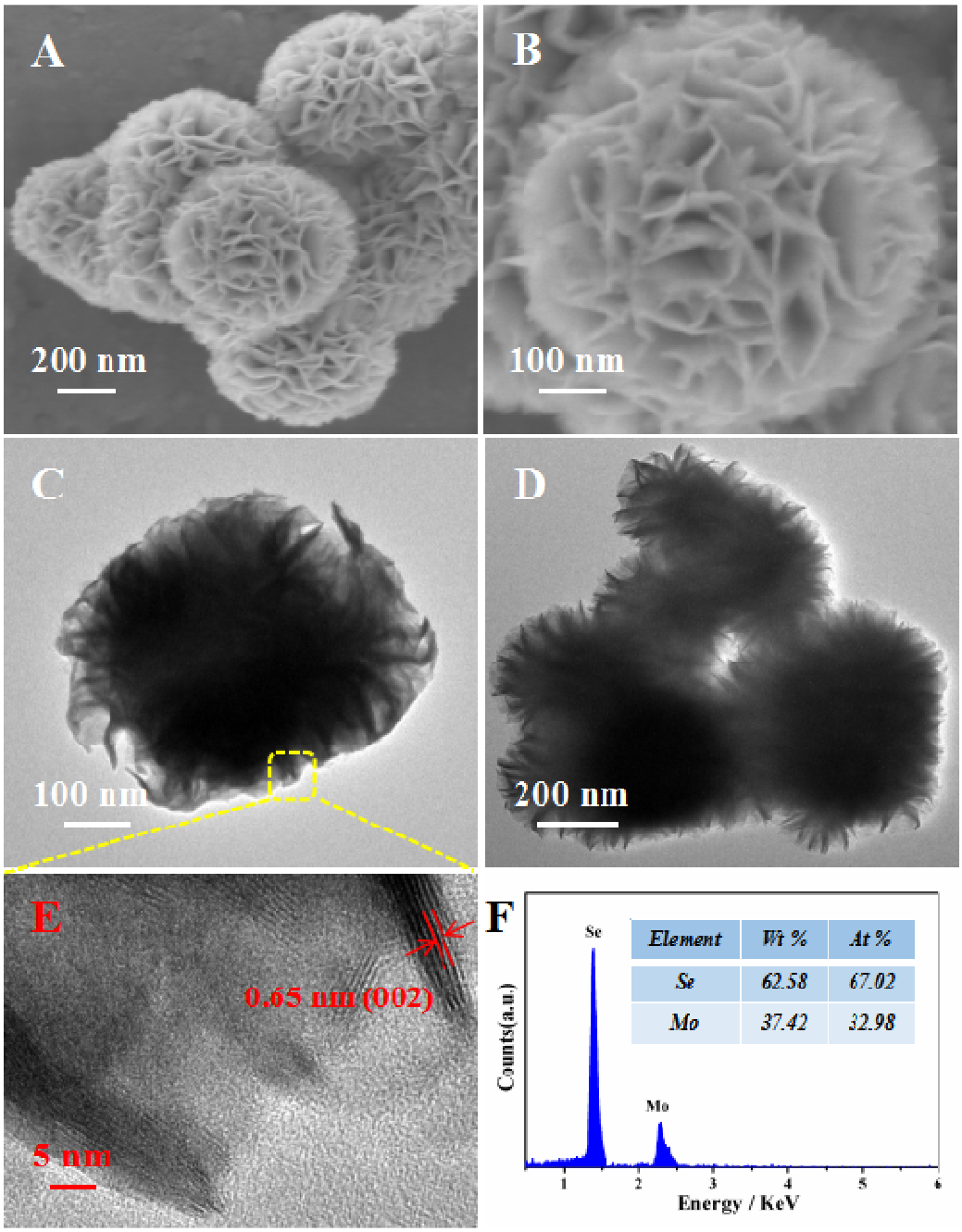

Fig 1. SEM (A, B), TEM (C, D), HRTEM (E) and EDX (F) images of the flower-like $MoSe_2$ microspheres.

It has been confirmed that the NG-metal nanoparticles hybrid not only can facilitate electron transfer but also can enhance the intrinsic electrocatalytic activity of NG through electronic structure modification, which is propitious to the fabrication of

View Article Online
DOI: 10.1039/C8TB00061A

high-performance elelctrochemical biosensors.[44] Moreover, combinations of NG with metal particles will also continue to be fashionable due to the synergistic effects of combining materials. In this work, NG-AuNPs hybrids were prepared and characterized with SEM, TEM and HRTEM. Compared with the pristine GO (Fig. S1A), NG is nearly transparent layer with some wrinkled and folded regions (Fig. 2A). Two-dimensional structure of graphene is well kept after dopping with N. The TEM of NG in Fig. 2B shows that the NG is highly transparent with silk-like parts, which is thinner than original GO (Fig. S1B). Fig S1C shows the SEM of NG-AuNPs. Numerous aggregated AuNPs evenly distribute on NGs, which will provide large surface area and good conductivity (Fig. 2C). From Fig. 2D, an interplanar spacing of ~0.24 nm is observed, corresponding to the D-spacing of the (111) plane of the Au.[37]

View Article Online
DOI: 10.1039/C8TB00061A

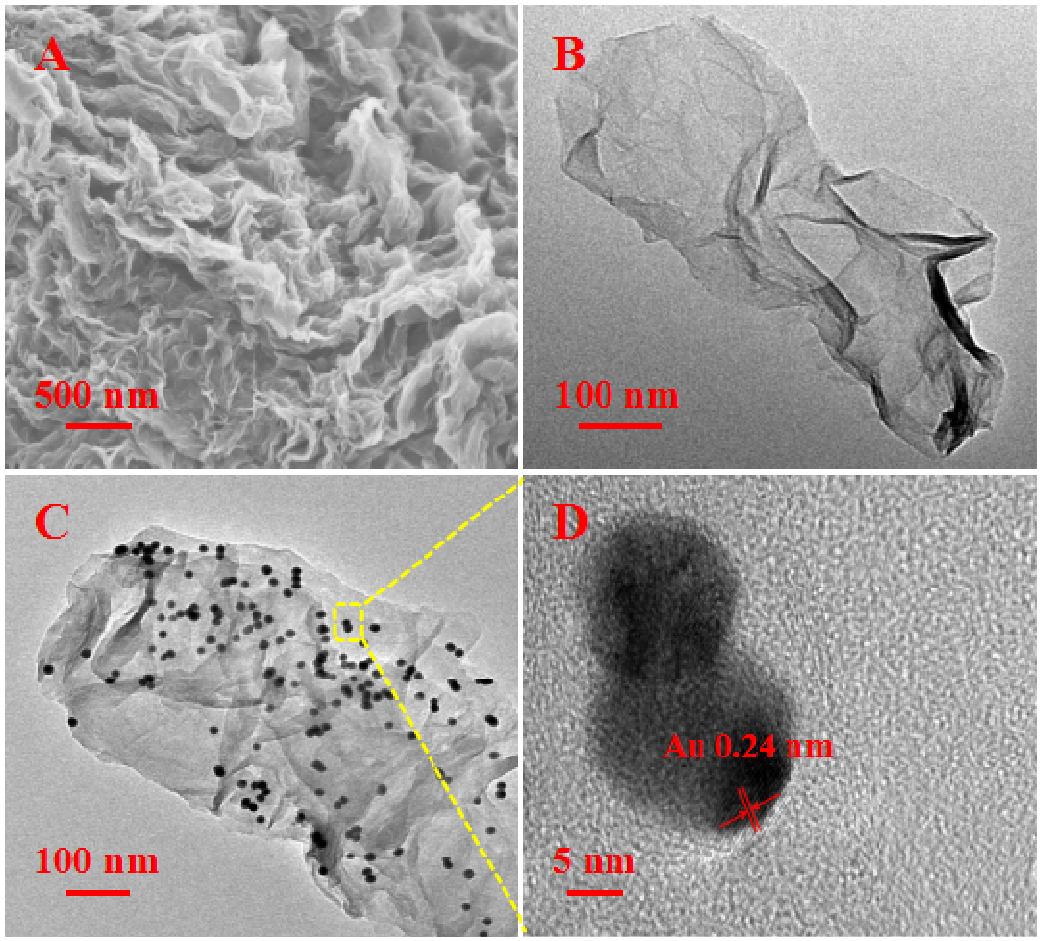

Fig 2. (A) SEM and (B) TEM of NG; (C) TEM and (D) HRTEM images of NG-AuNPs.

X-ray powder diffractometer (XRD) was used to characterize the as-prepared samples. As shown in Fig. 3A, the diffraction peaks of $MoSe_2$ microspheres focus at 13.46°, 26.43°, 33.57°, 41.09°, 46.04° and 54.72° (2θ), corresponding to (002), (004), (100), (103), (105) and (110) planes of the 2H-$MoSe_2$ phase, respectively, which are perfectly consistent with standard card (JCPDS Card, No.29-0914).[43] There are no other impurity peaks, suggesting high purity of the samples. The differences of structure among GO, NG and NG-AuNPs samples are shown in Fig. 3B. A diffraction peak of C (001) plane can be indexed to the GO (black line) located at 11.15° (2θ).[45]

View Article Online
DOI: 10.1039/C8TB00061A

The peak at 24.04° for the NG sample (blue line) is assigned to the hexagonal graphite structure C (002). As for the NG-AuNPs sample (red line), the diffraction peaks of 37.54° (111), 43.84° (200), 64.08° (220) and 76.85° (311) are characteristic of the crystalline nanodomains of AuNPs. Fig. 3C shows Raman spectrum of the $MoSe_2$ sample. The $MoSe_2$ shows characteristic E_{1g}, A_{1g} (out-of-plane), E^1_{2g} (in-plane) and A^2_{2u} modes at 169, 242, 285 and 352 cm^{-1} respectively.[46] Fig. 3D compares the Raman spectra of GO (black line), NG (blue line) and NG-AuNPs (red line), revealing two peaks at around 1349.66 and 1593.23 cm^{-1}, assigning to *D* and *G* bands, respectively. The *D*-band is attributed to defect induced mode, and *G*-band is result of the vibration of sp^2-hybridized carbon atoms in a 2D hexagonal lattice.[47] Generally, the intensity ratios of *D* and *G* bands (I_D/I_G) reflect the degree of graphitization. The I_D/I_G ratio becomes smaller proves the higher graphitization degree. Herein, the I_D/I_G of GO, NG and NG-AuNPs are 0.79, 0.97 and 0.99, respectively. The results show that the destroys on the GR carbon skeleton, distortion degree and defect sites increase after N-doping. Chemical compositions and the valence states of these samples were further detected by XPS. From the XPS survey spectrum of $MoSe_2$ in Fig. 3E, the elements of Mo, Se, C and O, can be obviously observed. The C 1s peak at 283.13 eV comes from the pollution of environment. A small quantity of O is attributed to the adsorption of oxygen. As shown in Fig. S2A, the Mo $3d_{3/2}$ and Mo $3d_{5/2}$ peaks are found at 231.48 and 228.34 eV, which confirms the presence of +4 valence of molybdenum.[48] Fig. S2B shows the spectrum and binding energy of Se 3d at 55.29 and 54.43 eV, corresponding to the Se $3d_{3/2}$ and Se $3d_{5/2}$, which confirms the

View Article Online
DOI: 10.1039/C8TB00061A

existance of -2 valence of Se.[48] XPS survey spectrum of GO (black line), NG (blue line) and NG-AuNPs (red line) are exhibited in Fig. 3F. The wide-scan XPS of GO shows the existence of carbon and oxygen elements. In contrast to the GO, the XPS survey spectra of NG clearly shows one new element, which can be ascribe to the N1s. The decreased O signal on the NG compared with GO as a result of the O release during the doping procedure. The bonding structures of C atoms in the pristine GO (Fig. S3A) and NG (Fig. S3B) are detected by high-resolution XPS. The C 1s band can be fitted into six peaks at 284.54, 285.20, 286.01, 286.67, 288.12 and 289.32 eV, corresponding to C=C, C-N, C-C, C-O, C=O/C=N, O-C=O. The presence of C-N and C=N peaks confirms successful N doping.[49] As shown in Fig. S3C, the high-resolution N 1s band demonstrates the presence of four formations of N (oxidized N, pyridinic N, pyrrolic N and graphitic N) which are located close to 397.30, 398.49, 399.55, and 401.08 eV. In addition, Fig. S3D shows the spectrum of Au 4f, and the binding energies at 84.07 and 87.77 eV belong to Au $4f_{7/2}$ and $4f_{5/2}$, respectively,[37] further indicating AuNPs have been availably assembled on the NG.

View Article Online
DOI: 10.1039/C8TB00061A

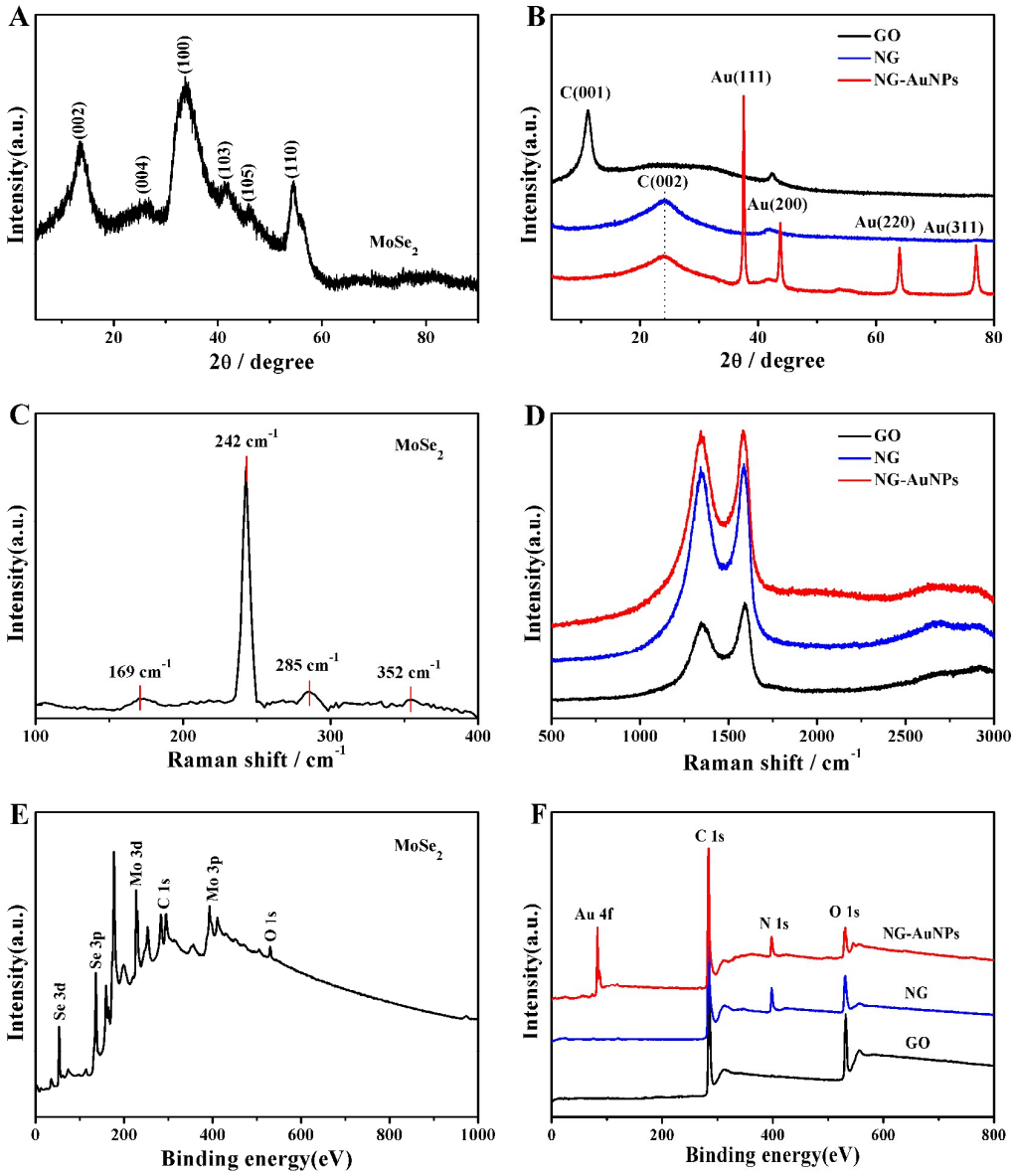

Figure 3. XRD pattern of $MoSe_2$ microspheres (A), and GO, NG, NG-AuNPs (B); Raman spectra of $MoSe_2$ microspheres (C), GO, NG, NG-AuNPs (D); XPS survey spectra of $MoSe_2$ microspheres (E), GO, NG, NG-AuNPs (F).

3.2 Electrochemical characterization

In order to characterize every immobilization step of the sensing interface, the cyclic voltammetric (CV) and electrochemical impedance spectroscopy (EIS) were

View Article Online
DOI: 10.1039/C8TB00061A

performed in 0.1 M PBS containing 10 mM potassium ferricyanide and 0.1 M potassium chloride solution. As displayed in Fig. 4A, the bare GCE demonstrates two reversible redox peaks (curve a). When $MoSe_2$ microspheres are decorated on GCE, a clearly increased peak current (curve b) is gained, suggesting $MoSe_2$ has a good electron transfer capacity. With the AuNPs electrodeposited on the $MoSe_2$/GCE (curve c), the peak current greatly increases because AuNPs can facilitate the electron transfer. Nevertheless, as displayed in Fig. 4B, the peak current response dramatically decreases after capture DNA is immobilized on electrode (curve d). This is because the introduction of DNA increases the steric hindrance and its the negatively charges repellent $[Fe(CN)_6]^{3-/4-}$. After incubating with MCH to obstruct nonspecific binding sites, an obvious decrease in current is got (curve e). Subsequently, the redox peak current further reduces after incubating of target miRNA on the electrode (curve f) because of more negative charges on it. However, current response apparently increases after the immobilization of the DNA-linked NG-AuNPs hybrid (curve g). After assistance DNA is applied on the electrode (curve h), current response reduces. These results show the electrochemical biosensor is successfully prepared.

Since EIS is a powerful and sensitive technique for researching interface properties of electrode surface,[15] it was used to investigate fabrication process of biosensor. The inset of Fig. 4C shows the Randles's equivalent circuit. R_{ct} reflects the change of the electrode interface. In Fig. 4C, GCE reveals one small semicircle domain (curve a). Compared with the bare GCE, R_{ct} of $MoSe_2$/GCE (curve b) and AuNPs/$MoSe_2$/GCE (curve c) sequentially decrease, illustrating rapid electron

View Article Online
DOI: 10.1039/C8TB00061A

transfer process. However, the electrode incubated with capture DNA causes a clearly increase of R_{ct} (curve d). With the sequential assembly of MCH (curve e) and target miRNA (curve f), the R_{ct} increases in turn, due to MCH blocking nonspecific binding sites and oligonucleotides showing a negatively charged interface. Nevertheless, after the immobilization of the NG-AuNPs hybrid (curve g), a smaller R_{ct} is observed, indicating its good conductivity. The R_{ct} value increases after assembling assistance DNA. The result are in good agreement with CV. Fig. S4 shows the effective surface areas and the amplification effect of materials (see supporting information).

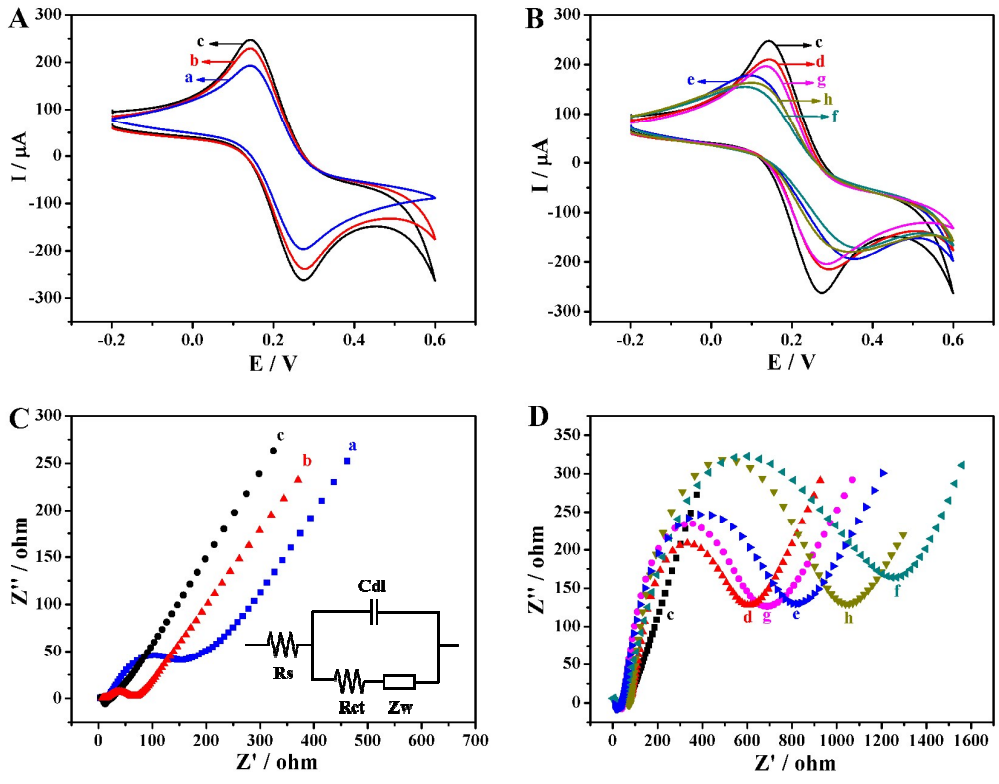

Fig 4. CV (A, B) and EIS (C, D) of different electrodes: GCE (a); $MoSe_2$/GCE (b); AuNPs/$MoSe_2$/GCE (c); capture probe/AuNPs/$MoSe_2$/GCE (d); MCH/capture probe/AuNPs/$MoSe_2$/GCE (e); miRNA/MCH/capture probe/AuNPs/$MoSe_2$/GCE (f);

View Article Online
DOI: 10.1039/C8TB00061A

DNA-linked NG-AuNPs/miRNA/MCH/capture probe/AuNPs/$MoSe_2$/GCE (g); assistance DNA/DNA-linked NG-AuNPs/miRNA/MCH/capture probe/AuNPs/$MoSe_2$/GCE (h).

3.3 Optimization

Some important parameters including incubation time of miRNA and pH of testing solution were optimized. As shown in Fig. 5A, electrochemical response gradually increases with incubation time increasing, and then the signal begins to level off after 60 min, suggesting the saturated binding is reached between the miRNA and capture probe. The pH of buffer solution also influences the performance of the proposed sensor. Differential pulse voltammetry (DPV) measurements were taken in 10 mM PBS. The maximum DPV signal is acquired at pH 8.0 (Fig. 5B). Consequently, pH 8.0 is chosen as the optimal pH in this experiment.

3.4 Comparison experiment

In order to prove the key role of NG-AuNPs hybrids, two types of modified electrodes were prepared: hemin/assistance DNA/DNA-linked AuNPs hybrids/miRNA/MCH/capture probe/AuNPs/$MoSe_2$/GCE (curve a) and hemin/ assistance DNA/DNA-linked NG-AuNPs/miRNA/MCH/capture probe/AuNPs/$MoSe_2$/GCE (curve b). Comparing curve a with b, the response remarkable increases may be due to the following reasons: first, numerous aggregated AuNPs evenly distributing on GNs may provide large surface area and enhance

View Article Online
DOI: 10.1039/C8TB00061A

conductivity, which not only can improve the immobilized amount of DNA, but also can enhance the catalytic activity.[31] Second, NG-AuNPs composites with good biocompatibility can provide more active sites for the immobilization of hemin/G-quadruplex. It is propitious to amplify electrochemical signal. From Fig. 5D, there is no electrochemical signal when the aptasensor is incubated with 25 mM HEPES buffer solution (200 mM NaCl and 1% DMSO, pH 8.0) (curve a). When 20 mM KCl is added in buffer solution, the signal also is hardly observed (curve b). Nevertheless, a weak peak can be observed after the addition of 50 μM hemin into the buffer solution (curve c). When 20 mM KCl and 50 μM hemin (curve d) were added, significant DPV peak current is obtained, due to the oxidation of hemin. These results illustrate the electrochemical signal of the biosensor is ascribed to redox reaction of hemin.

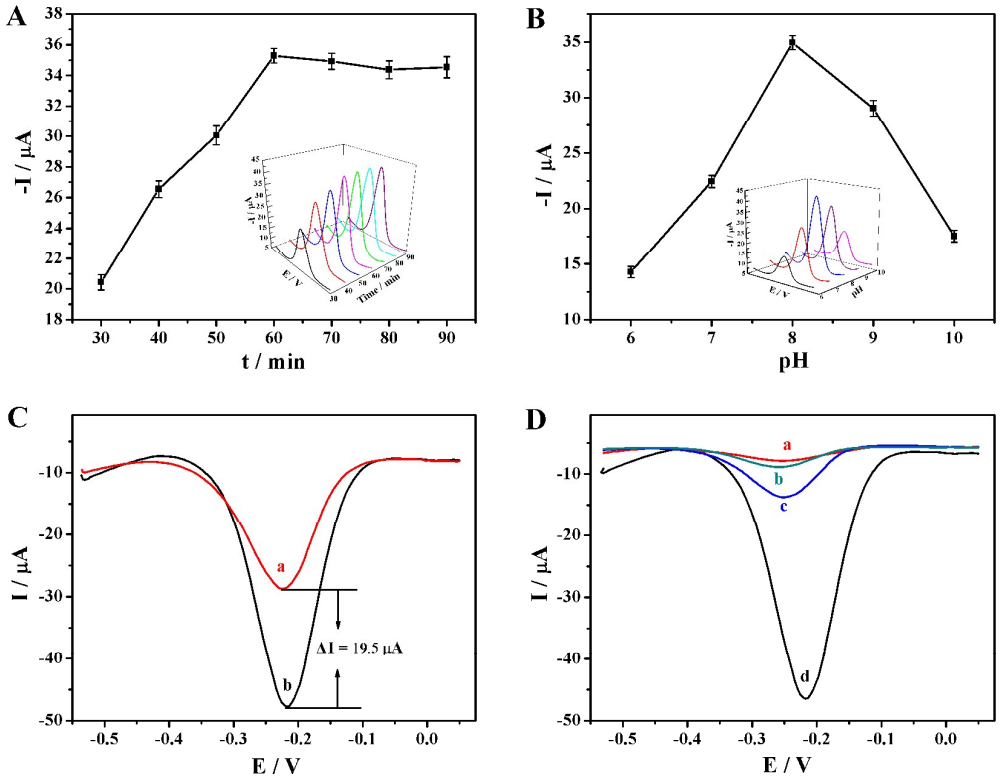

View Article Online
DOI: 10.1039/C8TB00061A

Fig. 5. The effect of miRNA incubation time (A) and pH (B); (C) DPV curves of different electrodes: hemin/assistance DNA/DNA-linked AuNPs/miRNA/MCH/capture probe/AuNPs/$MoSe_2$/GCE (a) and hemin/assistance DNA/DNA-linked NG-AuNPs/miRNA/MCH/capture probe/AuNPs/$MoSe_2$/GCE (b); (D) DPV responses of 20 mM KCl + 50 μM hemin (a), 20 mM KCl (b), 50 μM hemin (c), both 20 mM KCl and 50 μM hemin (d) in 25 mM HEPES buffer solution (200 mM NaCl and 1% DMSO, pH 8.0).

3.5 Analytical performance

Under the optimized condition, the aptasensor was used to determine miRNA. Fig. 6A shows DPV responses gradually enhances with increasing levels of analyte.[41] There is an excellent linear range of 10 fM-1 nM and regression equation is I(μA) = -5.99 log(c/M) -94.50 (I and c represent the peak current and miRNA concentration) (R = 0.996). Detection limit (LOD) is 0.17 fM (S/N=3). A comparison of analytical performance of our work with other methods is summarized in Table S1, which indicates that our assay has larger linear range and lower LOD, which is due excellent electrochemical properties of NG-AuNPs and large amount of immobilized hemin/G-quadruplexes. To satisfy the real sample analysis, miRNA was also detected in dilute blood. A linear range of 50 fM-1 nM was obtained with the regression equation of I(μA) = -4.82 log(c/M) - 78.50 (R = 0.990). LOD was 0.32 fM (S/N=3).

View Article Online
DOI: 10.1039/C8TB00061A

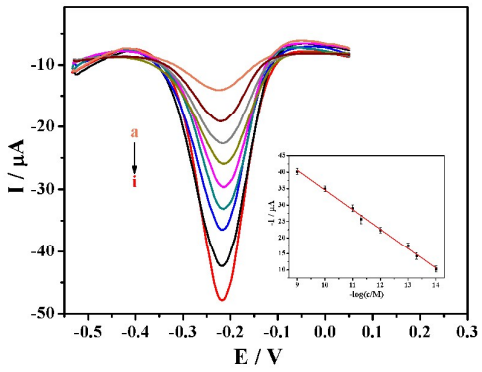

Fig. 6. DPV of different concentrations of miRNA-21 (a-i: 0, 1.0×10^{-14}, 5.0×10^{-14}, 1.0×10^{-13}, 1.0×10^{-12}, 5.0×10^{-12}, 1.0×10^{-11}, 1.0×10^{-10}, 1.0×10^{-9} M). Inset shows the calibration curve.

3.6 Selectivit and stability

To further evaluate the selectivity and specificity of developed biosensor, different miRNA sequences were detected. Fig. 7A shows significant changes of current response when tmRNA and non-complementary RNA are added compared to the blank test. Complementary sequence shows the biggest DPV response.[35] That of smRNA is approximately 15% of that of complementary miRNA. The result indicated that this strategy has outstanding selectivity toward miRNA-21 detection. We also evaluated the reproducibility and stability of the aptasensor. The DPV currents were recorded from five modified electrodes under identical conditions. RSD of 3.2% was obtained, illustrating good reproducibility. Additionally, five biosensors were independently kept under 4 °C for one week and measured the same analyt per days. As shown in Fig. 7B, the current responses have no obvious change, indicating good stability.

View Article Online
DOI: 10.1039/C8TB00061A

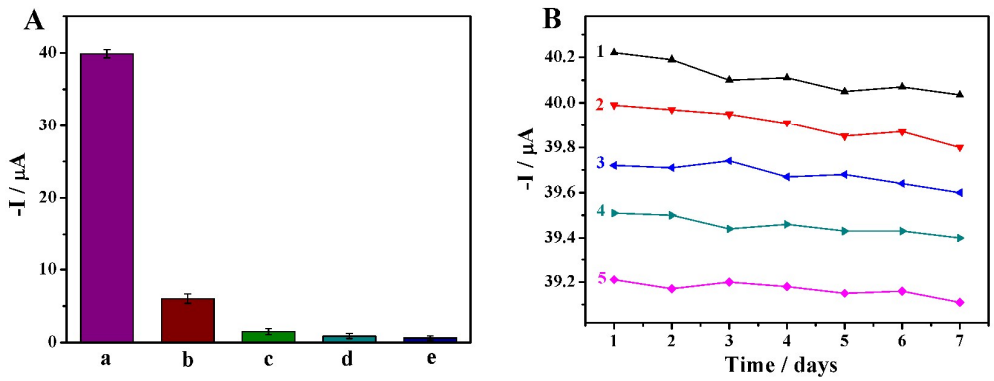

Figure 7. (A) Selectivity of the electrochemical biosensor. The different miRNA-21 sequences: complementary miRNA (a), smRNA (b), tmRNA (c) and non-complementary RNA (d), the blank test (e); (B) Signal intensities of the five modified electrodes (a-e) were obtained within two weeks.

3.7 Real sample analysis

For validating applicability of proposed assay, the recovery experiments were performed. Serum samples of patients were obtained from the affiliated hospital of Xinyang Normal University. After being settled for 2.5 h, the supernatants were extracted and then centrifuged at 3000 rpm three times for further purification. 0.1 mL obtained serum sample was then added to 1.0 mL PBS. Subsequently, the serum sample was detected by using the developed biosensor and the RT-PCR method, respectively. As shown in Table S2. The results obtained with the proposed biosensor are in good agreement with that obtained by qRT-PCR. All these experiments were performed in compliance with the relevant laws and institutional guidelines and the ethics committee that approved these experiments was the Institutional Review Board of the affiliated hospital of Xinyang Normal University. Informed consent was also

View Article Online
DOI: 10.1039/C8TB00061A

given by every participant.

4. Conclusion

In this work, an enzyme-free and ultrasensitiv supersandwich-type biosensor is fabricated based on NG-AuNPs and hemin/G-quadruplexe. This sensing platform possesses some fine characteristics: firstly, $MoSe_2$ and NG-AuNPs provid big specific surface area and excellent conductivity; secondly, NG-AuNPs hybrids can provide more active sites for the immobilization of probe DNA and hemin/G-quadruplex; thirdly, the sandwich structure can effecitvely enhance electrochemical performance. Finally, dual amplification processes are relatively less expensive and simple because it avoids the use of enzyme. Thus, it can eliminate the unfavorable factors of the involvement of enzyme and successfully assay the miRNA from real samples.

Acknowledgments

This work was supported by the National Natural Science Foundation of China (21475115), the Program for University Innovative Research Team of Henan (15IRTSTHN001), the Henan Provincial Science and technology innovation team (C20150026), the Nanhu Scholars Program of XYNU, the Nanhu Scholars Program for Young Scholars of XYNU, the Natural Science Foundation of Henan Province (162300410230) and the Henan Science and Technology Cooperation Project (172106000064).

View Article Online
DOI: 10.1039/C8TB00061A

References

1 D. Quiat and E. N. Olson, *J. Clin. Invest.* 2013, **123**, 11.

2 R. X. Leng, H. F. Pan, W. Z. Qin, G. M. Chen and D. Q. Ye, *Cytokine Growth F. R.* 2011, **22**, 141.

3 M.D. Jansson and A.H. Lund, *Mol. Oncol.* 2012, **6**, 590.

4 S.H. Chan, C.W. Wu, A.F.Y. Li, C.W. Chi, W.C. Lin, *Anticancer. Res.* 2008, **28**, 907.

5 Z. Zhang, Z. Li, C. Gao, P. Chen, J. Chen, W. Liu, S. Xiao, H. Lu, *Lab. Investig.* 2008, **88**, 1358.

6 S. Wang, S. Bi, Z. Wang, J. Xia, F. Zhang, M. Yang and Y. Xia, *Chem. Commun.* 2015, **51**, 7927.

7 W. F. Fang, W. J. Chen and J. T. Yang, *Sens. Actuators. B.* 2014, **192**, 77.

8 Y. Fu, T. Chen, G. Wang, T. Gu, C. Xie, J. Huang, X. Li, S. Best and G. Han, *J. Mater. Chem. B.* 2017, **5**, 7133.

9 P. Khandelwal and P. Poddar, *J. Mater. Chem. B.* 2017, **5**, 9055.

10 J. Huang, L. Ye, X. Gao, H. Li, J. Xu and Z. Li, *J. Mater. Chem. B.* 2015, **3**, 2395.

11 A. Zengin, U. Tamer and T. Caykara, *J. Mater. Chem. B.* 2015, **3**, 306.

12 X. Cao, Y. Shan, L. Tan, X. Yu, M. Bao, W. Li and H. Shi, *J. Mater. Chem. B.* 2017, **5**, 5983.

13 O. Adegoke and E. Y. Park, *J. Mater. Chem. B.* 2017, **5**, 3047.

14 H. L. Shuai, K. J. Huang, L. L. Xing and Y. X. Chen, *Biosens. Bioelectron.* 2016, **86**, 337.

15 H. L. Shuai, K. J. Huang, W. J. Zhang, X. Cao and M. P. Jia, *Sens. Actuators. B.*

View Article Online
DOI: 10.1039/C8TB00061A

2017, **243**, 403.

16 Y. X. Chen, W. J. Zhang, K. J. Huang, M. Zheng and Y. C. Mao, *Analyst.* 2017, **142**, 4843.

17 X. Li, F. Zheng and R. Ren, *Chem. Commun.* 2015, **51**, 11976.

18 H. Xu, C. Xue, R. Zhang, Y. Chen, F. Li, Z. Shen and Z. S. Wu, *Sens. Actuators. B.* 2017, **243**, 1240.

19 T. T. Nguyen, K. T. L. Trinh, W. J. Yoon, N. Y. Lee and H. Ju, *Sens. Actuators. B.* 2017, **242**, 1.

20 Y. X. Chen, K. J. Huang, F. Lin and L. X. Fang, *Talanta.* 2017, **175**, 168.

21 W. Shen, H. Deng and Z. Gao, *J. Am. Chem. Soc.* 2012, **134**, 14678.

22 H. L. Shuai, X. Wu, K. J. Huang and Z. B. Zhai, *Biosens. Bioelectron.* 2017, **94**, 616.

23 Y. X. Chen, K. J. Huang, L. L. He and Y. H. Wang, *Biosens. Bioelectron.* 2018, **100**, 274.

24 X. Hun, G. Xie and Luo, X. *Chem. Commun.* 2015, **51**, 7100.

25 J. Zhang, C. Li, X. Zhi, G. A. Ramón, Y. Liu, C. Zhang and D. Cui, *Anal. Chem.* 2015, **88**, 1294.

26 W. Xu, S. Dai, X. Wang, X. He, M. Wang, Y. Xi and C. Hu, *J. Mater. Chem. B.* 2015, **3**, 5777.

27 K. J. Huang, Y. J. Liu and Q. F. Zhai, *J. Mater. Chem. B.* 2015, **3**, 8180.

28 H. L. Shuai, K. J. Huang, Y. X. Chen, L. X. Fang and M. P. Jia, *Biosens. Bioelectron.* 2017, **89**, 989.

View Article Online
DOI: 10.1039/C8TB00061A

456 29 S.J. Deng, Y. Zhong, Y.X. Zeng, Y.D. Wang, Z.J. Yao, F. Yang, S.W. Lin, X.L.
457 Wang, X.H. Lu, X.H. Xia, J.P. Tu, *Adv. Mater.* 2017, 1700748.
458 30 H.T. Wang, D.S. Kong, P. Johanes, J.J. Cha, G. Zheng, K. Yan, N. Liu, Y. Cui,
459 *Nano Lett.* 2013, **13**, 3426.
460 31 D.S. Kong, H.T. Wang, J.C. Judy, P. Mauro, J.K. Kristie, J. Yao, Y. Cui, *Nano Lett.*
461 2013, 13, 1341.
462 32. Y. Tao, Y. H. Lin, J. S. Ren and X. G. Qu, *Biomaterials.* 2013, **34**, 4810.
463 33. J. J. Yang, J. T. Cao, Y. L. Wang, H. Wang, Y. M. Liu, and S. H. Ma, *J.*
464 *Electroanal. Chem.* 2017, **787**, 88.
465 34. X. X. Zeng, S. S. Ma, J. C. Bao, W. W. Tu, and Z. H. Dai, *Anal. Chem.* 2013, **85**,
466 11720.
467 35 G. Xiang, D. Jiang, F. Luo, F. Liu, L. Liu and X. Pu, *Sens. Actuators. B.* 2014, **195**,
468 515.
469 36 W. S. Hummers Jr and W. S. Offeman, *J. Am. Chem. Soc.* 1958, **80**, 1339.
470 37 M. Chen, C. Hou, D. Huo, J. Bao, H. Fa and C. Shen, *Biosens. Bioelectron.* 2016,
471 **85**, 684.
472 38 L. Lu, C. Liu, T. Kang, X. Wang, G. Guo and W. Miao, *Sens. Actuators. B.* 2018,
473 **255**, 35.
474 39 Z. Zhou, W. Wei, Y. Zhang and S. Liu, *J. Mater. Chem. B.* 2013, **1**, 2851.
475 40 K. J. Huang, Y. J. Liu, H. B. Wang, Y. Y. Wang and Y. M. Liu, *Biosens. Bioelectron.*
476 2014, **55**, 195.
477 41 H. L. Shuai, X. Wu and K. J. Huang, *J. Mater. Chem. B.* 2017, **5**, 5362.

View Article Online
DOI: 10.1039/C8TB00061A

42 E. Xiong, X. Zhang, Y. Liu, J. Zhou, P. Yu and J. Chen, *Anal. Methods.* 2016, **8**, 2106.

43 D. Sun, S. Feng, M. Terrones and R.E. Schaak, *Chem. Mater.* 2015, **27**, 3167.

44 Y. H. Wang, K. J. Huang and X. Wu, *Biosens. Bioelectron.* 2017, **97**, 305.

45 N. M. Galdino, G. S. Brehm, R. Bussamara, W. D. Gonçalves, G. Abarca and J. D. Scholten, *J. Mater. Chem. B.* 2017, **5**, 9482.

46 D. J. Late, S. N. Shirodkar, U. V. Waghmare, V. P. Dravid and C. N. R. Rao, *ChemPhysChem.* 2014, **15**, 1592.

47 Z. Wang, X. Xiong, L. Qie and Y. Huang, *Electrochim. Acta.* 2013, **106**, 320.

48 H. Tang, K. Dou, C. C. Kaun, Q. Kuang and S. Yang, *J. Mater. Chem. A.* 2014, **2**, 360.

49 L. L. Xing, K. J. Huang, S. X. Cao and H. Pang, *Chem. Eng. J.* 2018, **332**, 253.